Electric Field Inside a Gas Cavity Formed at a Solid-Solid Dielectric Interface Stressed with HV Impulses

T. Wong, I. Timoshkin, S. MacGregor, M. Wilson and M. Given
Department of Electronic and Electrical Engineering
The University of Strathclyde
Glasgow, Scotland
timothy.wong@strath.ac.uk

***Abstract*— Interfaces between solid dielectric materials may exhibit lower breakdown strength compared to that associated with bulk breakdown of solid materials. A reason for such reduction is the presence of gas cavities which are formed at the interface. When the solid-solid interface is subjected to impulsive electrical stress, the enhanced electric field inside cavities may result in the development of initial (partial) discharges. This may ultimately lead to breakdown across the interface, resulting in the catastrophic failure of the entire insulation system. Therefore, it is paramount to understand the field distribution and ionisation processes within interfacial cavities, such that the behavior and strength of the insulation system can be fully predicted. The present paper considers a gas-filled cavity formed between poorly-conducting solids, subjected to a transient external electric field. The corresponding boundary value problem is defined and analytically solved, obtaining closed form solutions for the electric field distribution inside and around an isolated cavity. Results from model validation and intra-cavity field enhancement are presented, as well as brief discussion of other possible applications and future model extensions.**

Keywords—dielectric breakdown; solid-solid interfaces; impulsive breakdown; analytical model; field enhancement

I. INTRODUCTION

In high voltage and pulsed power systems, the physical construction and coordination of insulation is imperative for the prevention of unwanted electrical breakdown. In many such systems, joints between solid dielectric materials may be unavoidable, and could pose a significant risk to the safety and integrity of the system. Solid-solid interfaces are known to exhibit lower breakdown strength compared to their bulk counterparts [1,2], especially in cases where the field component parallel to the interface is significant. Yet, the reasons for a reduced breakdown strength and the factors affecting the evolution of interfacial discharges have not yet been fully established.

Several studies, including [3,4], have provided evidence that solid-solid interfacial breakdown is linked to the breakdown of gas cavities formed between the two dielectrics in contact (illustrated in Fig. 1). The unavoidable surface roughness of each material leads to the creation of microscale voids at the interface. This type of solid-solid interface is typically found in dry-mate connectors, and the interfacial voids are thus gas-filled. Field enhancement caused by the mismatch of permittivity, or possibly by space charge accumulation [5], may induce a gaseous discharge through the string of voids, and this has been identified as one of the causes of reduced interfacial strength. Subsequently, this theory formed the basis of investigations for more recent works, such as in a series of linked studies by Hasheminezhad et al. [3,4] and Kantar et al. [6-8]. These works focused on the mechanical parameters of an interface that may influence the cavity size and/or distribution. A comprehensive model in [6,7] summarises these findings by blending approaches from the fields of tribology and high voltage engineering. Through this model, clear links between surface roughness parameters, composite elastic modulus, interfacial contact pressure and the reduced breakdown strength of solid interfaces were established.

It is notable, however, that the majority of studies conducted to date on the subject are performed under steady-state AC or DC conditions, generally focusing their efforts on mechanical parameters and its effects on interfacial voids. Therefore, there exists a need to quantify and extend these findings to transient conditions, as well as to better include electrical parameters, particularly to meet the needs of pulsed power applications. In this paper, a mathematical model is presented for a single isolated gas-filled cavity at a solid-solid interface, under the application of an impulsive uniform electric field of a double-exponential form. It is assumed that the impulsive field with magnitude of E_0 is generated between two parallel electrodes, with the interface positioned perpendicular to the electrodes. Fully closed form solutions for the transient pre-breakdown electric field inside and around the gas cavity are obtained, under the consideration that all materials, both solid dielectrics and the gas, are poorly conducting, allowing an arbitrary choice for both the relative permittivity and the electrical conductivity of all components under analysis.

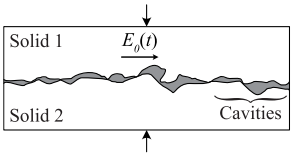

Fig. 1. Illustration depicting cavities formed at the rough interface between two solid insulating materials.

II. Mathematical Model

A. Problem Geometry

For the model developed and presented in this work, a single cavity is approximated by a simple spheroidal inclusion of radius r_1, encased in a solid bulk material and subject to an external time-dependent potential $\varphi_0(r, \theta, t)$. An additional layer of radius $r_2 > r_1$ is included in the present model, approximating a layer of altered material parameters arising from, for example, a wet contact or carbonisation from previous repeated (partial) discharges. The entire geometry is assumed to be symmetrical about the direction of the applied field, as such, this simple model does not consider interfaces which are formed between two different materials. A diagram of the full geometry is shown in Fig. 2. Each poorly conducting region is defined by a parameter pair of relative permittivity and electrical conductivity in S/m, (ε, σ). These are subscripted *g, l* and *b* for the gas, the altered layer, and bulk, respectively. The potential $\varphi_0(r, \theta, t)$ can be written in spherical coordinates as (1).

$$\varphi_0(r, \theta, t) = -E_0(t) r \cos\theta \tag{1}$$

with $E_0(t)$ being the field magnitude in V/m, r and θ the spatial coordinates, and t being time.

B. Boundary Value Problem Definition

The solution methodology follows that of [9], with the exception that no assumptions are made for (ε, σ) pairs, allowing for a fully generalised solution. For pre-breakdown conditions assuming negligible space charge, the potential field $\varphi(r, \theta, t)$ must follow Laplace's equation, which is expanded to spherical coordinates in (2). For the brevity of expressions, functional notation is omitted except where it enhances clarity.

$$\nabla^2\varphi = \frac{1}{r^2}\frac{\partial}{\partial r}\left(r^2\frac{\partial\varphi}{\partial r}\right) + \frac{1}{r^2\sin\theta}\frac{\partial}{\partial\theta}\left(\sin\theta\frac{\partial\varphi}{\partial\theta}\right) = 0 \tag{2}$$

Note that there is no dependence on the azimuthal angle Φ due to the imposed condition of rotational symmetry. It can be shown that general solutions of the potential φ in each dielectric layer (*g,l,b*) from (2) take the form of the expressions in (3).

$$\begin{aligned} \varphi_g &= A_g(t) r\cos\theta \\ \varphi_l &= \left(A_l(t) r + B_l(t)\frac{1}{r^2}\right)\cos\theta \\ \varphi_b &= \left(A_b(t) r + B_b(t)\frac{1}{r^2}\right)\cos\theta \end{aligned} \tag{3}$$

where $A(t)$ and $B(t)$ are time-dependent coefficients, once again carrying subscripts identifying their respective layer. To arrive at a particular solution, appropriate boundary conditions must be applied. In this case, one must firstly ensure continuity of the electric potential across dielectric layers; and secondly, that current continuity is also satisfied. Mathematically, the boundary conditions are written as (4) and (5), respectively.

$$\begin{aligned} \varphi_g(r_1) &= \varphi_l(r_1) \\ \varphi_l(r_2) &= \varphi_b(r_2) \end{aligned} \tag{4}$$

$$\boldsymbol{J}_g\cdot\hat{\boldsymbol{n}} + \partial_t(\boldsymbol{D}_g\cdot\hat{\boldsymbol{n}})\big|_{r_1} = \boldsymbol{J}_l\cdot\hat{\boldsymbol{n}} + \partial_t(\boldsymbol{D}_l\cdot\hat{\boldsymbol{n}})|_{r_1}$$

$$\boldsymbol{J}_l\cdot\hat{\boldsymbol{n}} + \partial_t(\boldsymbol{D}_l\cdot\hat{\boldsymbol{n}})|_{r_2} = \boldsymbol{J}_b\cdot\hat{\boldsymbol{n}} + \partial_t(\boldsymbol{D}_b\cdot\hat{\boldsymbol{n}})|_{r_2} \tag{5}$$

Here, $\boldsymbol{J} = \sigma\boldsymbol{E}$ is the current density in A/m², $\boldsymbol{D} = \varepsilon\boldsymbol{E}$ is the electric flux density in C/m² and $\hat{\boldsymbol{n}}$ is the unit normal. To reach a self-consistent solution in presence of the external field, a final boundary condition prescribing the field as r becomes much larger than that of the cavity dimensions must be applied, as in (6).

$$\lim_{r\to\infty}\varphi_b = \varphi_0 \tag{6}$$

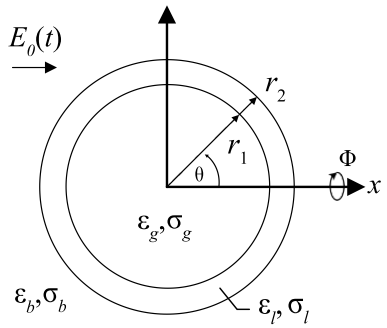

Fig. 2. Diagram of spheroidal cavity geometry. Each layer considers arbitrary (ε, σ) pairs, and is rotationally symmetric about the x axis ($y = 0$). $E_0(t)$ is the external electric field.

C. Boundary Value Problem Solution Method

The solutions for the coefficients of (3) are found by prescribing the boundary conditions of (4), (5) and (6). To facilitate this process, all associated equations are transformed into the complex frequency domain by application of the Laplace transform. In the context of the present boundary value problem, this requires solely the transformation of the time dependent functions $f(t)$ and their first derivatives, such that $f(t) \rightarrow f(s)$ and $\partial_t f(t) \rightarrow sf(s)$. The resulting set of equations are solved algebraically to yield s-domain solutions for the coefficients $A(s)$ and $B(s)$ as a function of the s-transformed external field $E_0(s)$ for each layer. A time-domain solution is reconstructed by choice of $E_0(s)$ and application of the inverse transform. This is demonstrated for the case of a 1.2/50 μs lightning impulse in section III.

III. Model Results and Validation

A. Double-exponential Response

For the purposes of model validation, an applied impulsive field generated from a pair of plane-parallel electrodes is considered. Analytically, the double-exponential representation is assumed for the applied field following (7).

$$E_0(t) = \frac{A_0 U_0}{d}\left(e^{-\alpha t} - e^{-\beta t}\right) \tag{7}$$

where U_0 is the peak voltage in V, d is the gap separation in m and A_0, α, β are wave-shaping parameters. Following the solution process outlined in section II, closed-form time-domain expressions are obtained for all coefficients and, consequently, for all fields. Due to the extent of the mathematical forms, this brief paper only presents the final time-domain expressions. It is shown that the coefficients exhibit a complex quad-exponential form, following (8) to (12).

$$A_l(t) = \frac{-3\sigma_b A_0 U_0}{d(2\sigma_b+\sigma_l)\left[\tau_1\tau_2 + 2\left(\frac{r_1}{r_2}\right)^3 m\tau_3\tau_4\right]} \times \left[e^{-\frac{t}{\tau_5}}\left(\frac{\beta-\alpha}{\eta}\right)\left(1-\frac{\tau_b+\tau_1}{\tau_5}+\frac{\tau_b\tau_1}{\tau_5^2}\right) + e^{-\frac{t}{\tau_6}}\left(\frac{\beta-\alpha}{\lambda}\right)\left(1-\frac{\tau_b+\tau_1}{\tau_6}+\frac{\tau_b\tau_1}{\tau_6^2}\right) + \frac{e^{-\alpha t}}{\kappa}\left[1-\alpha(\tau_b+\tau_1)+\tau_b\tau_1\alpha^2\right] - \frac{e^{-\beta t}}{\xi}\left[1-\beta(\tau_b+\tau_1)+\tau_b\tau_1\beta^2\right]\right] \quad (8)$$

$$B_l(t) = \frac{-3r_1^3\sigma_b(\sigma_l-\sigma_g)A_0U_0}{d(2\sigma_b+\sigma_l)(2\sigma_l+\sigma_g)\left[\tau_1\tau_2 + 2\left(\frac{r_1}{r_2}\right)^3 m\tau_3\tau_4\right]} \times \left[e^{-\frac{t}{\tau_5}}\left(\frac{\beta-\alpha}{\eta}\right)\left(1-\frac{\tau_b+\tau_3}{\tau_5}+\frac{\tau_b\tau_3}{\tau_5^2}\right) + e^{-\frac{t}{\tau_6}}\left(\frac{\beta-\alpha}{\lambda}\right)\left(1-\frac{\tau_b+\tau_3}{\tau_6}+\frac{\tau_b\tau_3}{\tau_6^2}\right) + \frac{e^{-\alpha t}}{\kappa}\left[1-\alpha(\tau_b+\tau_3)+\tau_b\tau_3\alpha^2\right] - \frac{e^{-\beta t}}{\xi}\left[1-\beta(\tau_b+\tau_3)+\tau_b\tau_3\beta^2\right]\right] \quad (9)$$

$$B_b(t) = r_2^3[A_l(t)+E_0(t)] + B_l(t) \quad (10)$$

$$A_g(t) = A_l(t) + B_l(t)\frac{1}{r_1^3} \quad (11)$$

$$A_b(t) = -E_0(t) \quad (12)$$

whereby the relaxation time constants are given by (13).

$$\tau_b = \frac{\varepsilon_0\varepsilon_b}{\sigma_b},\ \tau_l = \frac{\varepsilon_0\varepsilon_l}{\sigma_l}$$
$$\tau_1 = \frac{2\varepsilon_l+\varepsilon_g}{2\sigma_l+\sigma_g}\varepsilon_0,\ \tau_2 = \frac{2\varepsilon_b+\varepsilon_l}{2\sigma_b+\sigma_l}\varepsilon_0$$
$$\tau_3 = \frac{\varepsilon_l-\varepsilon_g}{\sigma_l-\sigma_g}\varepsilon_0,\ \tau_4 = \frac{\varepsilon_b-\varepsilon_l}{\sigma_b-\sigma_l}\varepsilon_0$$
$$\tau_{5,6} = \frac{2}{\delta \mp \sqrt{\delta^2-4\gamma}} \quad (13)$$

And the constants δ, γ and *m* follow the expressions of (14).

$$\delta = \frac{(\tau_1+\tau_2)+2\left(\frac{r_1}{r_2}\right)^3 m(\tau_3+\tau_4)}{\tau_1\tau_2+2\left(\frac{r_1}{r_2}\right)^3 m\tau_3\tau_4}$$
$$\gamma = \frac{1+2\left(\frac{r_1}{r_2}\right)^3 m}{\tau_1\tau_2+2\left(\frac{r_1}{r_2}\right)^3 m\tau_3\tau_4}$$
$$m = \frac{(\sigma_l-\sigma_g)(\sigma_b-\sigma_l)}{(2\sigma_b+\sigma_l)(2\sigma_l+\sigma_g)} \quad (14)$$

Finally, the constants η, λ, κ and ξ relate to the time constants as shown in (15).

$$\eta = \left(\frac{1}{\tau_6}-\frac{1}{\tau_5}\right)\left(\alpha\beta-\frac{\alpha+\beta}{\tau_5}+\frac{1}{\tau_5^2}\right)$$
$$\lambda = \left(\frac{1}{\tau_5}-\frac{1}{\tau_6}\right)\left(\alpha\beta-\frac{\alpha+\beta}{\tau_6}+\frac{1}{\tau_6^2}\right)$$
$$\kappa = \frac{1}{\tau_5\tau_6}-\alpha\left(\frac{1}{\tau_5}+\frac{1}{\tau_6}\right)+\alpha^2$$
$$\xi = \frac{1}{\tau_5\tau_6}-\beta\left(\frac{1}{\tau_5}+\frac{1}{\tau_6}\right)+\beta^2 \quad (15)$$

The electric field is found by taking the gradient of (3), to yield (16). It can therefore be shown that the field inside the cavity is also uniform in nature.

$$\boldsymbol{E_g} = -A_g(t)\cos\theta\,\hat{\boldsymbol{r}} + A_g(t)\sin\theta\,\hat{\boldsymbol{\theta}} \quad (16)$$

B. Comparison to Simulation

To validate the developed analytical model, a direct comparison of the calculated field magnitude to that found through electrostatic simulation software was performed. For the purposes of demonstration, a 5 kV peak, 1.2/50 μs lightning impulse, following the IEC 60060 standard was chosen as the input voltage. Wave-shaping parameters for the analytical double-exponential waveform were computed using a particle-swarm like technique, resulting in values of $A_0 \sim 1.03$, $\alpha \sim 1.47\times10^4$ and $\beta \sim 2.47\times10^6$. These agree well with reported parameters computed in [10]. System geometrical and material properties were chosen to reflect the values of common insulators, while the cavity dimensions were based approximately on the known range of voids formed between engineering surfaces from contact studies [8]. The additional layer described in section II-A was set to possess slightly higher values for both (ε, σ) and was thin compared to the cavity length, while the gas cavity was set to (ε, σ) = (1,0). The full set of parameters are tabulated in Table 1.

Using the finite element field solver QuickField [11], an axisymmetric, transient electric model with geometry identical to that of Fig. 1 is simulated up to 20 μs with a time step of 0.1 μs. The resulting comparison between the intra-cavity field magnitude between computational and analytical models are presented in Fig. 3, for which excellent agreement is found.

TABLE I. MODEL PARAMETERS FOR VALIDATION

Param.	*Value*	*Param.*	*Value*	*Param.*	*Value*
U_0	5 kV	r_1	14 μm	σ_g	0 S/m
A_0	1.03	r_2	15 μm	σ_l	10^{-9} S/m
α	1.47×10^4	ε_g	1	σ_b	10^{-12} S/m
β	2.47×10^6	ε_l	4.5		
d	4 mm	ε_b	3.2		

C. Field Enhancement

The fully closed form nature of the expressions obtained in this paper enables full visualisation of the complete spatially-varying electric field in the vicinity of the cavity. Fig. 4 plots the field enhancement factor in the axisymmetric space, defined as the field magnitude normalised by the magnitude of the uniform external field, $E_0(t)$, at time t. The parameters are the same as those tabulated in Table 1, and the image was taken at the time at which the cavity field reaches its maximum, t_{peak}. Two limiting cases were additionally considered, both analytically and by numerical substitution. The first replaced the gaseous cavity with a highly conducting (metallic) sphere. In this case, a maximal field enhancement of 3 was found around the extremes of the inclusion surface in the direction of the applied field. In the second case, for a conducting bulk encasing a gaseous inclusion, the maximum field enhancement was found to occur internal to the cavity, with a value of 3/2. Both cases align with well-established factors for the field enhancement due to spherical dielectric inclusions.

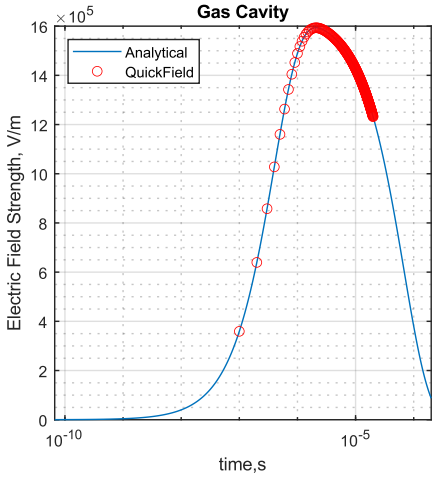

Fig. 3. Comparison of the cavity field strength given by (15) (solid line: —) and QuickField simulation output (open circles: o)

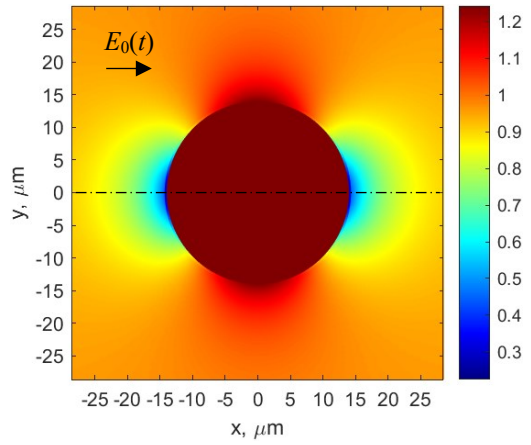

Fig. 4. Colour plot of the peak field enhancement factor, $E(t_{peak})/E_0(t_{peak})$, in the axisymmetric space (around $y = 0$), for the parameters given in Table 1. Under these conditions, maximum enhancement was found inside the cavity and normal to the applied field outside of the cavity.

IV. Conclusion

In the present study, an analytical approach has been applied to the practical problem of cavities formed between rough, poorly-conducting solid surfaces. A spheroidal cavity with a thin layer of higher conductivity and permittivity on the cavity wall was considered, subjected to a transient uniform field. The corresponding boundary value problem was defined and solved. Closed form solutions for the electric field in space and time have been demonstrated for impulsive energisation of a double-exponential form. The model was validated against simulations using the QuickField finite element solver, showing excellent agreement between computational and analytical results. The closed form nature of the present model, however, is able to produce transient field responses from arbitrary impulses at a fraction of the time compared to finite element methods. A similar model of an ellipsoidal cavity has also been successfully demonstrated and will be presented in future work. The model here is expected to become a part of larger study on solid-solid interfacial discharge under impulsive regimes, where it will be coupled with surface contact theory and ionisation processes. We remark, however, at the generality of the model, which may be of significant interest to several other fields including pulsed electric field (PEF) for biological applications, liquid dielectric breakdown involving gas-filled cavities or analysis of the influence of impulsive fields on complex particulates for decontamination studies.

References

[1] D. Fournier and L. Lamarre, "Effect of pressure and length on interfacial breakdown between two dielectric surfaces," IEEE Int. Symp. Electr. Insul., Baltimore, MD, USA, June 1992.

[2] R. Ross, "Dealing with interface problems in polymer cable terminations," IEEE Electr. Insul. Mag., vol. 15, pp. 5-9, July 1999.

[3] M. Hasheminezhad, E. Ildstad and A. Nysveen, "Breakdown strength of solid|solid interface," 10th IEEE Int. Conf. Solid Dielectr., Potsdam, Germany, July 2010.

[4] M. Hasheminezhad and E. Ildstad, "Application of contact analysis on evaluation of breakdown strength and PD inception field strength of solid-solid interfaces," IEEE Trans. Dielectr. Electr. Insul., vol. 19, pp. 1-7, February 2012.

[5] S. Delpino, et. al., "Polymeric HVDC cable design and space charge accumulation, Part 2: insulation interfaces," IEEE Electr. Insul. Mag., vol. 24, pp. 14-24, February 2008.

[6] E. Kantar, F. Mauseth and E. Ildstad, "Effect of pressure and elastic modulus on tangential breakdown strength of solid-solid interfaces," 34th Electr. Insul. Conf (EIC), pp. 431-435, Montréal, Qc, Canada, June 2016.

[7] E. Kantar, E. Ildstad and S. Hvidsten, "Effect of material elasticity on the longitudinal AC breakdown strength of solid-solid interfaces," IEEE Trans. Dielectr. Electr. Insul., vol. 26, pp. 655-663, April 2019.

[8] E. Kantar, S. Hvdisten, E. Ildstad and F. Mauseth, "A stochastic model for contact surfaces at polymer interfaces considering contact pressure, elasticity and surface roughness," Tribology Int., vol. 127, pp. 361-371, March 2018.

[9] I. Timoshkin, S. MacGregor, R. Fouracre, B. Crichton and J. Anderson, "Transient electrical field across cellular membranes: pulsed electric field treatment of microbial cells," J. Phys. D: Appl. Phys., vol. 39, pp. 596-603, January 2006.

[10] J. Wang and X. Zhang, "Double-exponential expression of lightning current waveforms," 4th Asia-pacific Conf. Environ. Electromag., CEEM, Dalian, China, August 2006.

[11] QuickField, Tera Analysis. Available: www.quickfield.com